Microstructural Evolution and Wear Dynamics of Al5052/Cenosphere Metal Matrix Composite Fabricated Through Compo-Casting Technique

Khursheed Ahmad Sheikh[1] · Fayaz Ahmad Mir[1]

Abstract The present study uses the compo-casting technique to fabricate cenosphere-reinforced Al5052 alloy. The wear tests were performed utilizing a pin-on-disk apparatus to examine the impact of load, sliding speed, and reinforcement wt.% on the wear rate. Employing response surface methodology (RSM), this research delves into the influences of load, sliding speed, and cenosphere content on the responses. As per the ANOVA analysis, load exhibited the most substantial effect. The ramp plots unveiled the optimal combination for minimizing wear rate identified as 200 rpm sliding speed, 10 N load, and 0 wt.% cenosphere reinforcement. The desirability plots reveal that the prediction value for wear rate is 0.7695 mm^3/Nm at a desirability of 96.8%. Incorporating cenosphere particles as reinforcement increased the wear resistance of the aluminum metal matrix composites (AMMCs).

Keywords Al5052 alloy · Compo-casting technique · Sliding wear · RSM

1 Introduction

Aluminum, possessing a lustrous, silver-white appearance, exhibits similar characteristics to other non-ferrous metals. Its highest level of functionality is attained by blending it with trace amounts of other metals, thereby boosting its strength and resilience without compromising its lightweight property. Moreover, alloying aluminum renders it exceptionally easy to machine [1]. The primary additive in aluminum 5052 (Al5052) alloy, belonging to the 5xxx series, is magnesium. Al5052 is classified as a non-heat treatable alloy and undergoes cold working processes to improve its strength. With remarkable properties and heightened fatigue resistance, Al5052 alloy is commonly utilized in structures subjected to repetitive vibrations [2]. The popularity of aluminum-based composites has surged owing to their remarkable strength and elevated modulus. These composites exhibit outstanding resistance to wear, a low coefficient of thermal expansion, resilience to high temperatures, and a notable capacity for damping [3]. Industries like automotive, aerospace, and marine are favoring advanced lightweight materials. AMMCs, with properties like durability and wear resistance, are set to meet industry demands. These composites can include various reinforcements for versatility [4, 5].

Metal matrix composites (MMCs) stand out as a promising category of materials due to their unique properties. While AMMCs offer a broad spectrum of reinforcement possibilities, their performance in tribological applications is impeded by their low hardness and limited wear resistance [6]. Optimal qualities and performance of metal matrix composites (MMCs) are achieved through meticulous selection of the reinforcing phase and careful consideration of processing techniques and parameters [7]. The utilization of aluminum metal matrix composites is on the rise across diverse technological applications, including vehicle pistons, and bicycle frames. These composites are appealing for a range of technical uses owing to their blend of high strength and exceptional corrosion resistance [8]. Zhiqiang et al. [9] examined the sliding wear characteristics of aluminum matrix composites reinforced with silicon. The results indicate that the composite exhibited a lower degree of weight reduction in comparison to the matrix alloy. Rao et al. [10] found that the wear rate of Al-Zn-Mg alloy composites

✉ Fayaz Ahmad Mir
  Fayaz_07phd19@nitsri.ac.in

1 Department of Mechanical Engineering, National Institute of Technology Srinagar, Srinagar, India

reinforced with SiCp increased with the applied pressure in the dry sliding wear tests at a consistent sliding speed. Das et al. [11] studied the wear behavior of SiC-reinforced aluminum alloy. Incorporating SiC particles as reinforcement increased the wear resistance of the aluminum metal matrix composites. Kishore et al. [12] examined Al5052 alloy reinforced with tungsten carbide. Experimental observations have shown that the wear resistance of Al 5052 alloy is improved by the addition of Tungsten carbide, especially as the weight percentage of reinforcement increases. Dey et al. [13] utilized the compo-casting technique to fabricate Al6061 alloys reinforced with cenosphere fly ash. The hybrid GRSM approach demonstrated exceptional efficacy, precision, and appropriateness in identifying the most favorable parameters for electrical discharge machining of Al6061/cenosphere AMCs.

Al5052 alloy-based metal matrix composites, applied in automobile and marine settings for their inherent wear resistance, face challenges due to limited hardness. This study explores the fabrication of Al5052/cenosphere composites using compo-casting, aiming to enhance wear resistance. The research focuses on refining wear process parameters through response surface methodology (RSM) for optimization. The investigation includes SEM analysis of worn surfaces, presenting an innovative approach to optimize wear-causing parameters not previously integrated in Al5052/cenosphere composites research.

2 Experimental

2.1 Material

Table 1 affords the chemical composition details of the Al5052 alloy. The compo-casting method was employed to manufacture both the Al5052 alloy and its composites. The creation of these composites involved using a Megatherm Induction Furnace from Werner Finley Pvt Ltd, along with the assistance of a mechanical stirrer. The process was initiated with the placement of aluminum alloy rods into a graphite crucible, subsequently heating

Table 1 Composition of Al5052 alloy

Element	Composition wt.%
Magnesium	2.3
Silicon	0.2
Copper	0.09
Iron	0.3
Manganese	0.02
Chromium	0.18
Zinc	0.01
Aluminum	Remainder

them in the induction electric furnace. The temperature was precisely regulated at 630 °C, ensuring the semi-solid condition of the Al5052 alloy. To induce a swirling motion in the molten metal, an electric motor-powered mechanical stir operated at a speed of 560 rpm. Before integration into the semi-solid melt, the cenosphere particles underwent preheating in a muffle furnace, reaching an approximate temperature of 255 °C. To maintain heat retention and impede rapid solidification, the iron mold was preheated to 655 °C. Following the preheating of cenosphere particles, they were introduced into the melt while stirring to ensure a uniform distribution within the aluminum matrix, as illustrated in the accompanying diagram. The partially solidified melt was subsequently poured into a pre-warmed iron mold and allowed to solidify at room temperature. This process was consistently applied to each composite variant, featuring different weight percentages of the reinforcement material (2 wt.%, 4 wt.%).

Test samples of circular cross sections measuring 12 mm in diameter and 6 mm in height are meticulously prepared for analysis through a sequence of steps. Initially, they undergo cutting via wire electric discharge machine employing molybdenum wire for the process. Subsequently, the samples undergo a grinding procedure utilizing emery sheets of various grades, reaching up to 2500 grades. Finally, conventional metallographic techniques are applied to polish the samples. To ensure a smooth and reflective surface finish, a paste containing alumina is coated onto the samples. Figure 1 illustrates a schematic depiction of the compo-casting process.

2.2 Wear Test

For the examination of dry sliding wear properties, a pin-on-disk tribometer was utilized (TR 20LE-PHM-400 model, DUCOM) in accordance with the ASTM standard G99-04. The wear samples were 10 mm in diameter and 6 mm in height. The initial step involved cleaning the specimen with acetone and determining its initial mass using a digital electronic balance. The pins were shaped using a machine and subsequently, a pin sample was securely clamped onto a rotating EN-32 steel disk (Ra = 0.43 μm) with a hardness of 65HRC [14]. The diameter of the pin is 8 mm, and the length of the pins is 30 mm. To stabilize the pin, a load was applied as a counterweight. Throughout the experiments, the track diameter was consistently maintained at 55 mm, while variations were introduced in load, sliding speed, and wt.% reinforcement. To continually assess wear levels, a Linear
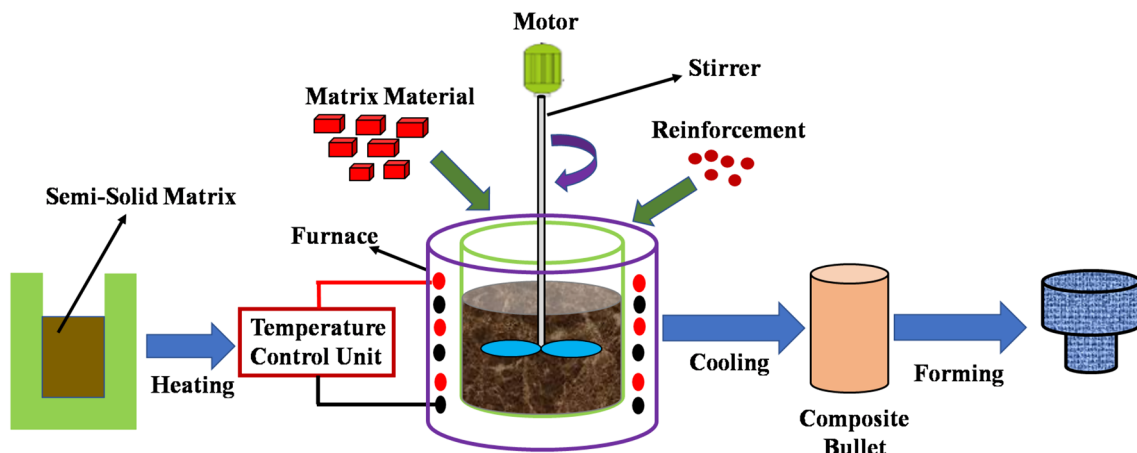
Fig. 1 Schematic depiction of the compo-casting process

Table 2 levels of parameters selected

Factors	Units	Levels		
		-1	0	1
Load	N	10	15	20
Sliding Speed	rpm	200	250	300
Reinforcement	wt.%	0	2	4

Fig. 2 XRD spectra of Al5052 alloy and its composites

Variable Differential Transformer (LVDT) was employed with a working range ± 2 mm, resolution ± 1 μm and least count 1 μm. The load induces the arm to sustain contact with the disk until the contact surface undergoes wear.

2.3 Optimization Method

The statistical analysis was carried out utilizing the Design Expert software. In this study, the RSM approach was applied to optimize the parameters influencing the dry sliding wear characteristics of both Al5052 alloy and its composites. The investigation concentrated on specific geometrical parameters, namely load, sliding speed, and wt.% reinforcement. The settings were selected based on three values outlined in Table 2. Experimental trials involved the manipulation of these geometrical parameters at three distinct levels.

3 Results and Discussion

3.1 X-ray Diffraction (XRD)

X-ray diffraction (XRD) analysis was conducted using CuK α radiation with a wavelength of 1.54 Å, covering a diffraction angle range from 20° to 90°. The XRD spectra of the synthesized samples are accessible in Fig. 2.
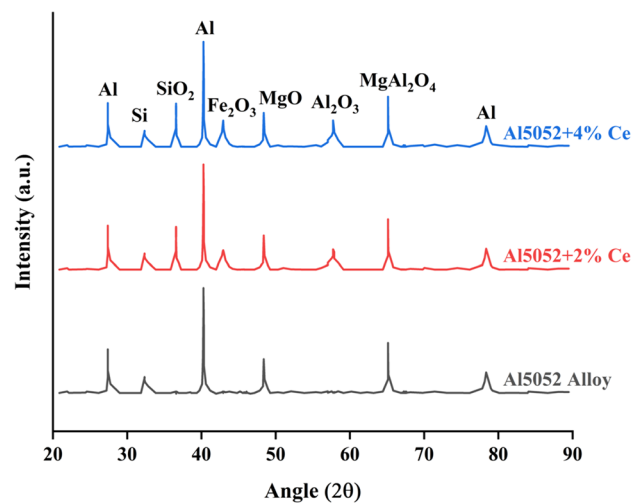
The investigation revealed the prominent presence of key components such as Al, Si, MgO, and $MgAl_2O_4$ in both the Al5052 alloys [15]. In addition to these peaks, SiO_2, Fe_2O_3, and Al_2O_3clearlyillustrate the stages of cenosphere particles within the composites [13]. As the amount of cenosphere particles in the Al5052 alloy grows, the intensities of the peaks also increase accordingly. Notably, no interfacial interactions are observed between the fly ash component and the matrix alloy material throughout the casting process. The compo-casting technique effectively prevents the formation of undesired intermetallic compounds [13]. The XRD analysis validates the absence of interfacial reactions at the aluminum-cenosphere contact.
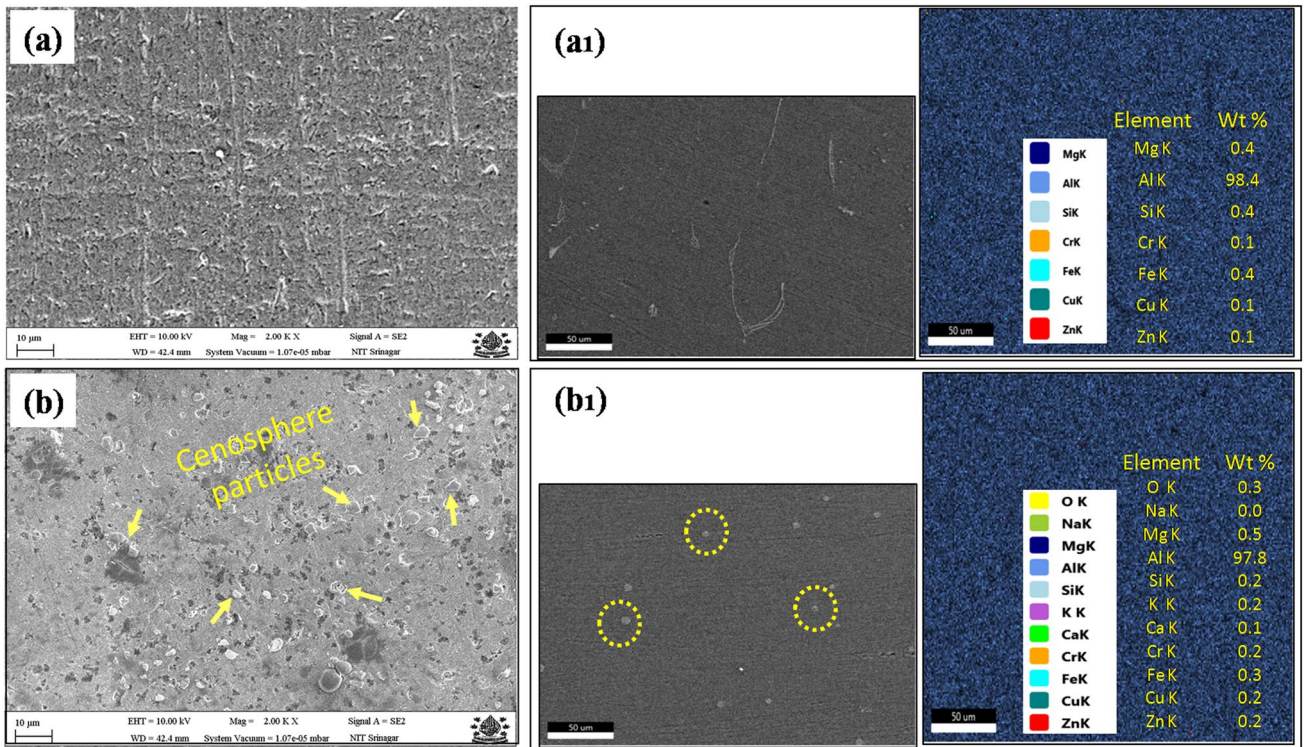
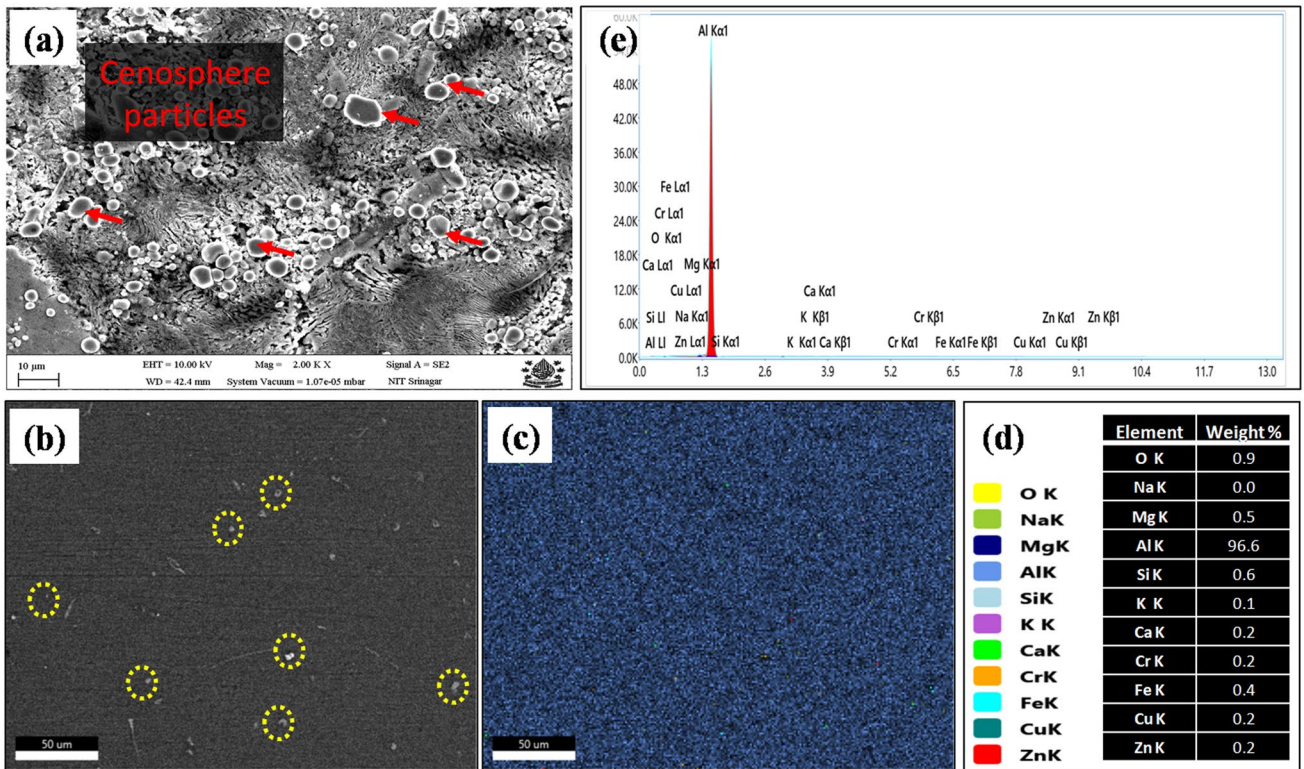**Fig. 3** SEM and EDS mapping of **a** Al5052 base alloy, **b** Al5052 + 2 wt.% Cenosphere

Fig. 4 SEM and EDS mapping of Al5052 + 4 wt.% Cenosphere

3.2 Microstructure Analysis

The test samples were 12 mm in diameter and 6 mm in height. Before SEM analysis, the samples were etched by modified Keller's reagent [16]. The scanning electron microscopy (SEM) images and EDS mapping described in Fig. 3 showcase the base Al5052 matrix alloy, and composites with 2% reinforcement, while as Fig. 4 depicts the microstructural analysis along with corresponding EDS mapping for the composite with 4% reinforcement. The SEM images of the Al5052/cenosphere composite reveal a uniform distribution of cenosphere particles within the alloy matrix, with the dispersion becoming more discernible with an increased concentration of fly ash particles. Notably, the micrographs exhibit an absence of voids, discontinuous phases, or slag inclusions. However, porosity is evident in the micrographs. This finding suggests that the selected compo-casting procedure successfully maintains the overall quality of the castings.

3.3 Response Surface Methodology (RSM)

A Central Composite Design (CCD) within RSM was applied to optimize the wear rate of Al5052/cenosphere composites. The experimental design adhered to the central composite design, encompassing 27 runs generated through Design Expert software to explore optimal outcomes. Independent parameter values were recorded during the wear test for various runs, as outlined in Table 3.

3.3.1 ANOVA for Wear Rate

Quadratic models were formulated to assess the wear rate, and their analysis was conducted using Fisher's F-test at a 95% confidence level in the Design Expert software. The models were deemed significant for evaluating the response variables. A Model F value of 126.15 indicates the statistical significance of the model, with a mere 0.01% probability that such a substantial F value could be attributed to random noise. P values below 0.05 suggest the statistical significance of model terms. The findings in Table 4 reveal that the load stands out as the most dominant parameter impacting the specific wear rate, followed by sliding speed, with reinforcement exhibiting the least significant effect.

Table 3 Designed matrix for different runs along with their response

| Run	Factor 1 A: load (N)	Factor 2 B: sliding speed (rpm)	Factor 3 C: reinforcement (wt.%)	Response 1 Wear rate (mm^3/Nm)
1	10	200	0	0.6973
2	10	200	2	0.7762
3	10	200	4	0.8362
4	10	250	0	0.9853
5	10	250	2	1.0862
6	10	250	4	1.2483
7	10	300	0	1.3981
8	10	300	2	1.4971
9	10	300	4	1.5194
10	15	200	0	1.5644
11	15	200	2	1.5845
12	15	200	4	1.5951
13	15	250	0	1.5995
14	15	250	2	1.6195
15	15	250	4	1.7611
16	15	300	0	1.8373
17	15	300	2	1.8812
18	15	300	4	1.9985
19	20	200	0	2.0662
20	20	200	2	2.1762
21	20	200	4	2.3851
22	20	250	0	2.4123
23	20	250	2	2.5364
24	20	250	4	2.6743
25	20	300	0	2.7532
26	20	300	2	2.8101
27	20	300	4	2.9712

In Table 5, it is evident that the disparities between adjusted R^2 and predicted R^2 are less than 0.2, indicating a robust concordance between the two R^2 values for the response. Adeq. Precision serves as a measure of the signal-to-noise ratio, with an ideal ratio exceeding 4. The ratio of 36.5875 signifies a satisfactory signal. ANOVA established empirical correlations for the wear rate by employing the crucial factors in a coded format. The equation grounded on real factors can be applied to predict the outcome for specific levels of each factor.

$$Wear\,Rate = 1.68 + 0.7078\,Load + 0.2769\,Sliding\,Speed + 0.0931\,Reinforcement$$

$$-0.0165\,Load * Sliding\,Speed + 0.0230\,Load * Reinforcement$$

$$+0.0010\,Sliding\,Speed * Reinforcement + 0.1082\,Load^2$$

$$+0.0279\,Sliding\,Speed^2 + 0.0204\,Reinforcement^2$$

(1)

Table 4 ANOVA for wear rate

Source	Sum of squares	DOF	Mean square	F value	p value	
Model	10.64	9	1.18	126.15	<0.0001	Significant
A-load	9.02	1	9.02	962.16	<0.0001	
B-sliding Speed	1.38	1	1.38	147.29	<0.0001	
C-reinforcement	0.1560	1	0.1560	16.64	0.0008	
AB	0.0033	1	0.0033	0.3482	0.5629	
AC	0.0063	1	0.0063	0.6758	0.4224	
BC	0.0000	1	0.0000	0.0013	0.9719	
A^2	0.0702	1	0.0702	7.49	0.0141	
B^2	0.0047	1	0.0047	0.4969	0.4904	
C^2	0.0025	1	0.0025	0.2676	0.6116	
Residual	0.1593	17	0.0094			
Cor total	10.80	26				

Table 5 Fit statistics for wear rate

	Standard Deviation	Mean	C.V. %	R^2	Adjusted R^2	Predicted R^2	Adeq. Precision
Wear Rate	0.0968	1.79	5.42	0.9852	0.9774	0.9626	36.5875
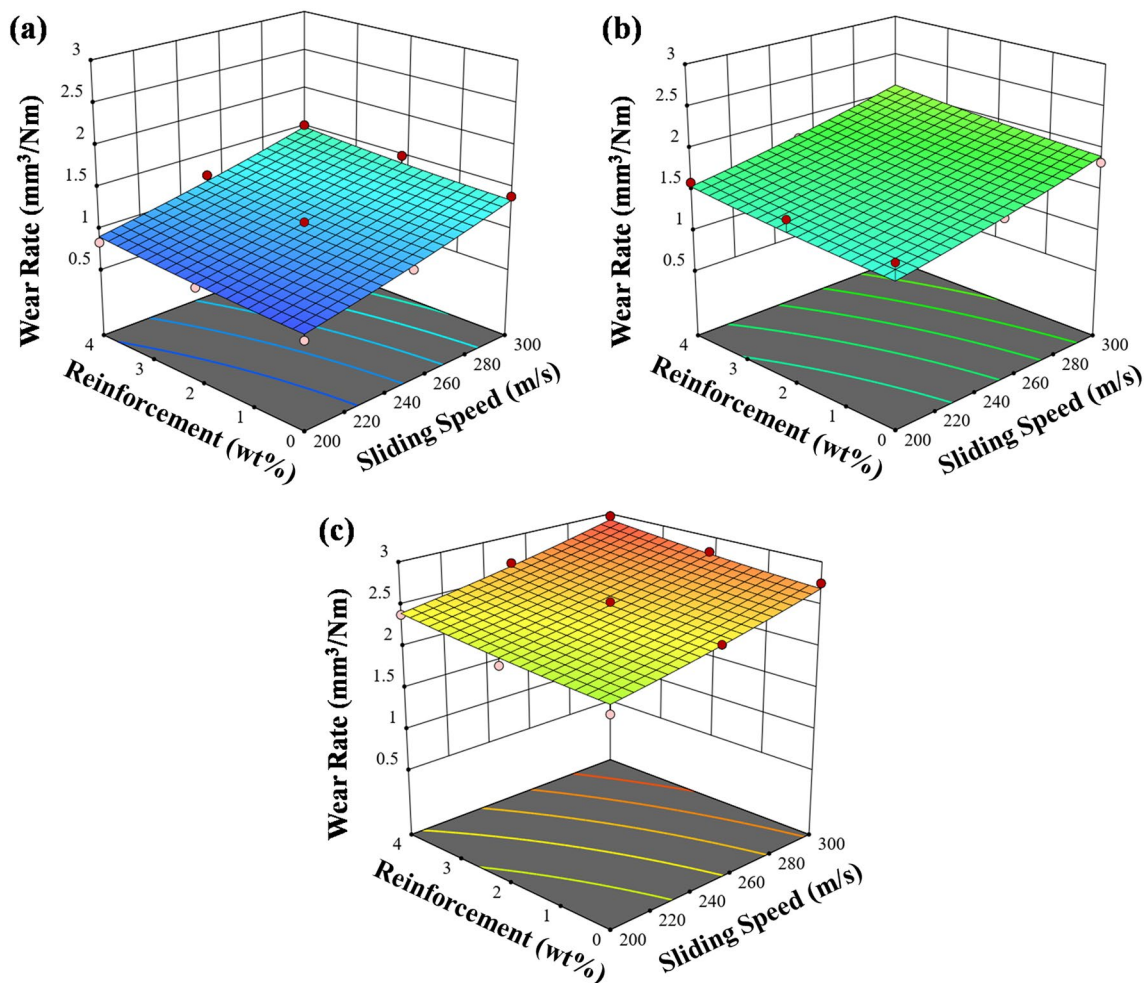
Fig. 5 3D surface plots for the wear rate at **a** 10 N load, **b** 15 N load, and **c** 20 N load

3.3.2 Effect of the Input Parameters on Wear Rate

Figure 5 displays 3D surface plots for wear rate at different loads. Increasing sliding speed and weight percent reinforcement leads to higher wear rates, indicating a positive correlation. This suggests that elevated sliding speeds and greater cenosphere reinforcement intensify material wear, possibly due to increased friction and surface interaction. This understanding is crucial for optimizing conditions in applications with Al5052/Cenosphere composites to minimize wear.

In Fig. 6, the 3D surface plots depict wear rate variations at different sliding speeds. As load and weight percent reinforcement increase, the wear rate also rises. This indicates that higher applied loads and increased reinforcement proportion result in an accelerated wear rate for the material. The correlation suggests that factors like heightened stress on the material and enhanced surface interaction contribute to the observed increase in wear.

Figure 7 presents 3D surface plots showing wear rate variations with different weight percentages of reinforcement. The observation indicates that increasing both load and sliding speed concurrently raises the wear rate. This suggests that higher loads and increased sliding speeds contribute to more significant wear, possibly due to heightened friction and added stress on the material. The 3D surface plots aid in visualizing the intricate relationship between these factors and the resulting wear rate.

Figure 8a demonstrates the disparity between predicted and actual values for output response, revealing a robust correlation between the model's generated values and the observed outcomes. If the points were aligned along a 45° angle to the actual values, any inaccuracies would be uniformly distributed across the model. In Fig. 8b, the normal
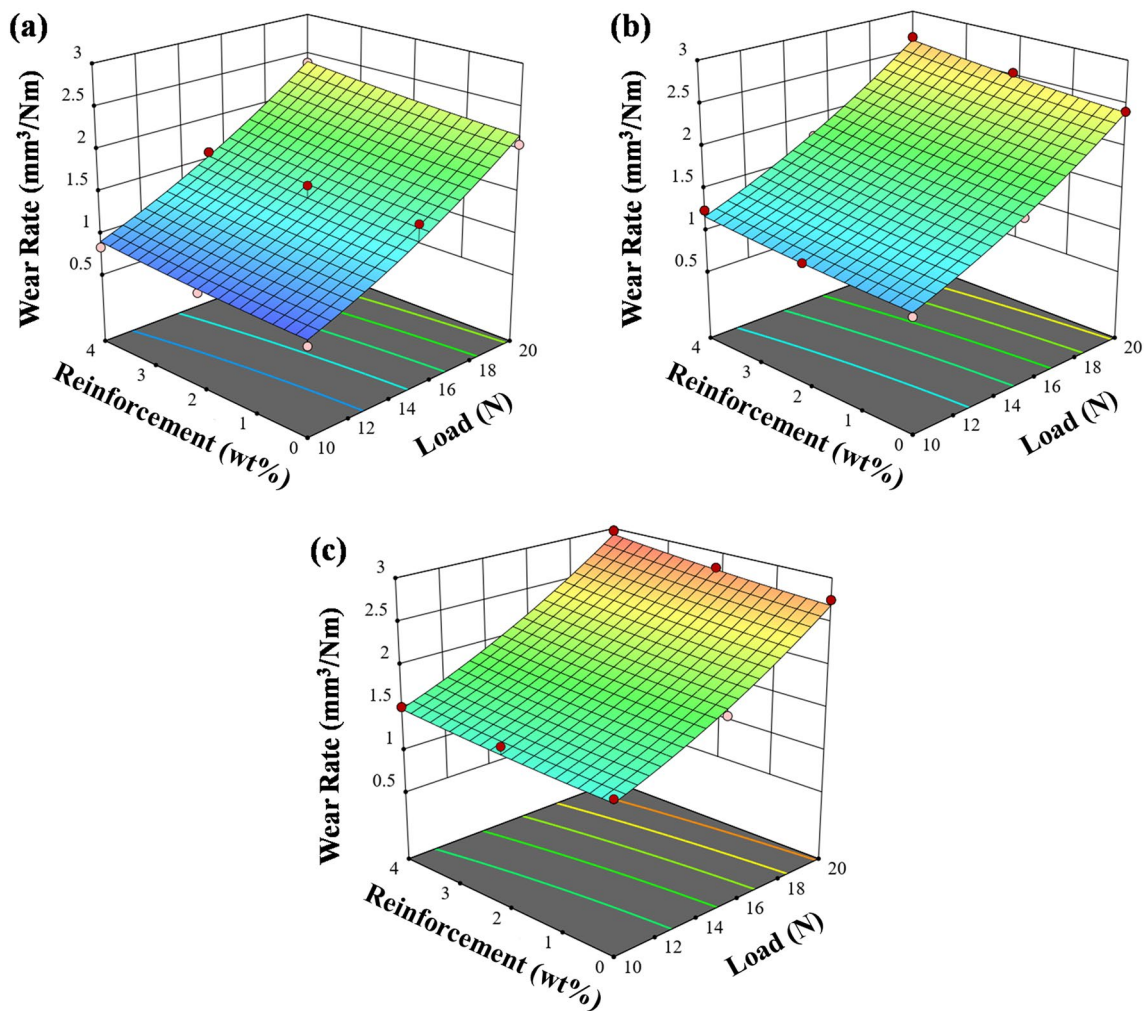

Fig. 6 3D surface plots for the wear rate at **a** 200 rpm sliding speed, **b** 250 rpm sliding speed, and **c** 300 rpm sliding speed
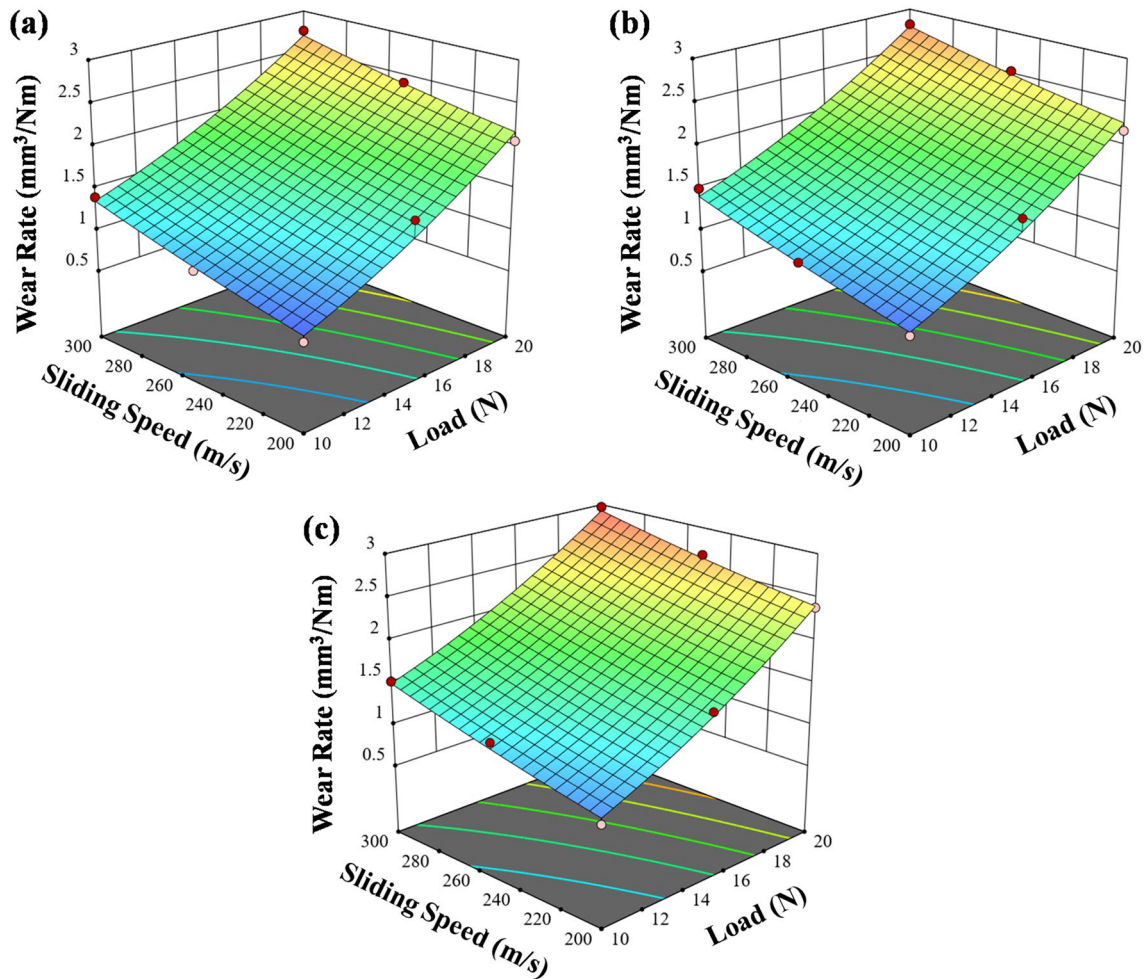
Fig. 7 3D surface plots for the wear rate **a** Al5052 alloy, **b** Al5052 + 2wt.% cenosphere and **c** Al5052 + 4 wt.% cenosphere

plot of residuals for the wear rate demonstrates that the residuals closely adhere to the normal probability line, indicating a normal distribution. This suggests that the terms within the regression model are both substantial and acceptable. Furthermore, Fig. 8c presents a plot of residuals against the fitted values of the wear rate, where the residuals exhibit a random distribution. The regression model proposed for the wear rate is deemed satisfactory. Figure 9a shows the outcomes of the multi-response optimization. The ramp charts reveal that the wear rate achieved optimization at a load of 10N, sliding speed of 200 rpm, and reinforcement of 0wt.% cenosphere particles. The optimal wear rate indicated is 0.707 mm^3/Nm. Figure 9b shows the desirability plots for wear rate. The plots reveal that the prediction value for wear rate is 0.7695 mm^3/Nm at a desirability of 96.8%.

An experimental confirmation test was carried out at the specified location to validate the proposed model, utilizing the process parameters recommended by the model. The wear rate for the specimen in the confirmation test was assessed, and the measured response were aligned within the 95% confidence interval of the projected response values. Notably, a minimal 2.86% percentage error was observed between the predicted and experimental values, underscoring a robust correlation as depicted in Table 6.

3.4 Worn Surfaces

Figures 10, 11 and 12 illustrate the microstructural analysis of the worn surfaces of Al5052 base alloy and its composite samples with 2% and 4% reinforcement, respectively. The wear test was conducted at the optimal level combination of
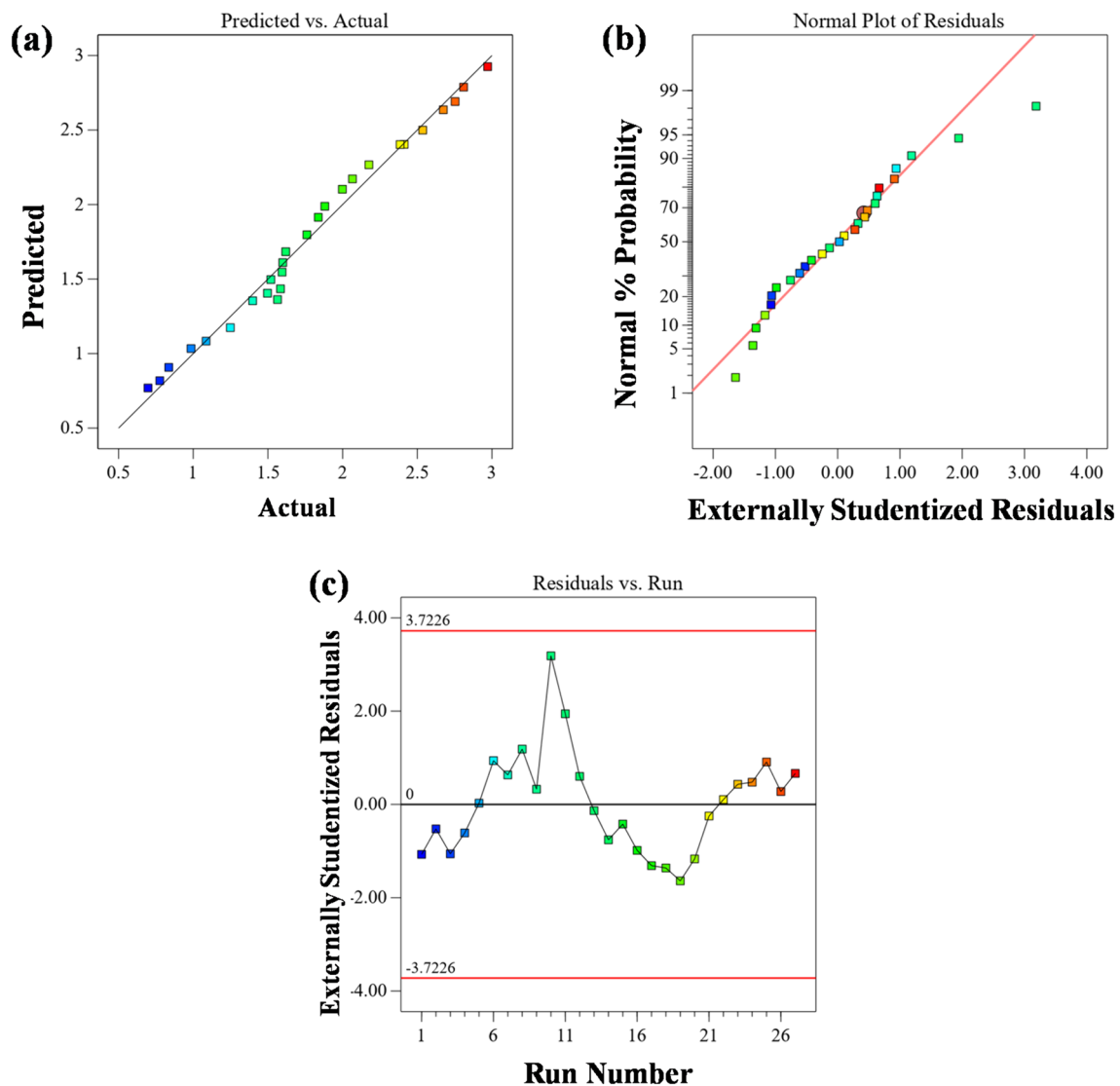
Fig. 8 **a** Predicted versus actual values, **b** Normal plot of residuals, and **c** Residuals versus run plot

parameters as 10 N load, 200 rpm sliding speed, and 0 wt.% reinforcement for minimum wear rate. The wear images reveal the scratches and surface irregularities of the optimized samples resulting from wear. Generally, indentations (grooves) are visible on the affected surface, likely caused by the plastic deformation of the AMC samples when sliding under dry conditions [11]. The plowing and delamination were the principal wear mechanisms at optimal conditions. The delamination of the layer is seen at the margins. Delamination on the edges can occur due to concentrated stress, where the material is more vulnerable to separation.

Figure 13 displays the 3D surface topography of the worn surfaces at optimized conditions. The Al5052 + 4%Cenosphere composite exhibited the lowest surface roughness, measured as Ra = 1.05 μm^{-1}, and the Al5052 + 2 wt.% Cenosphere composite exhibited Ra = 1.16 μm^{-1}. On the other hand, the Al5052 alloy showed the highest surface roughness among the tested materials, with a value of Ra = 1.346 μm^{-1}. This implies that the worn surfaces of Al5052 alloy had a rougher texture compared to the composites. Lower roughness values indicate better resistance to wear. Therefore, under the specified conditions, the Al5052 + 4 wt.% Cenosphere performed better in terms of
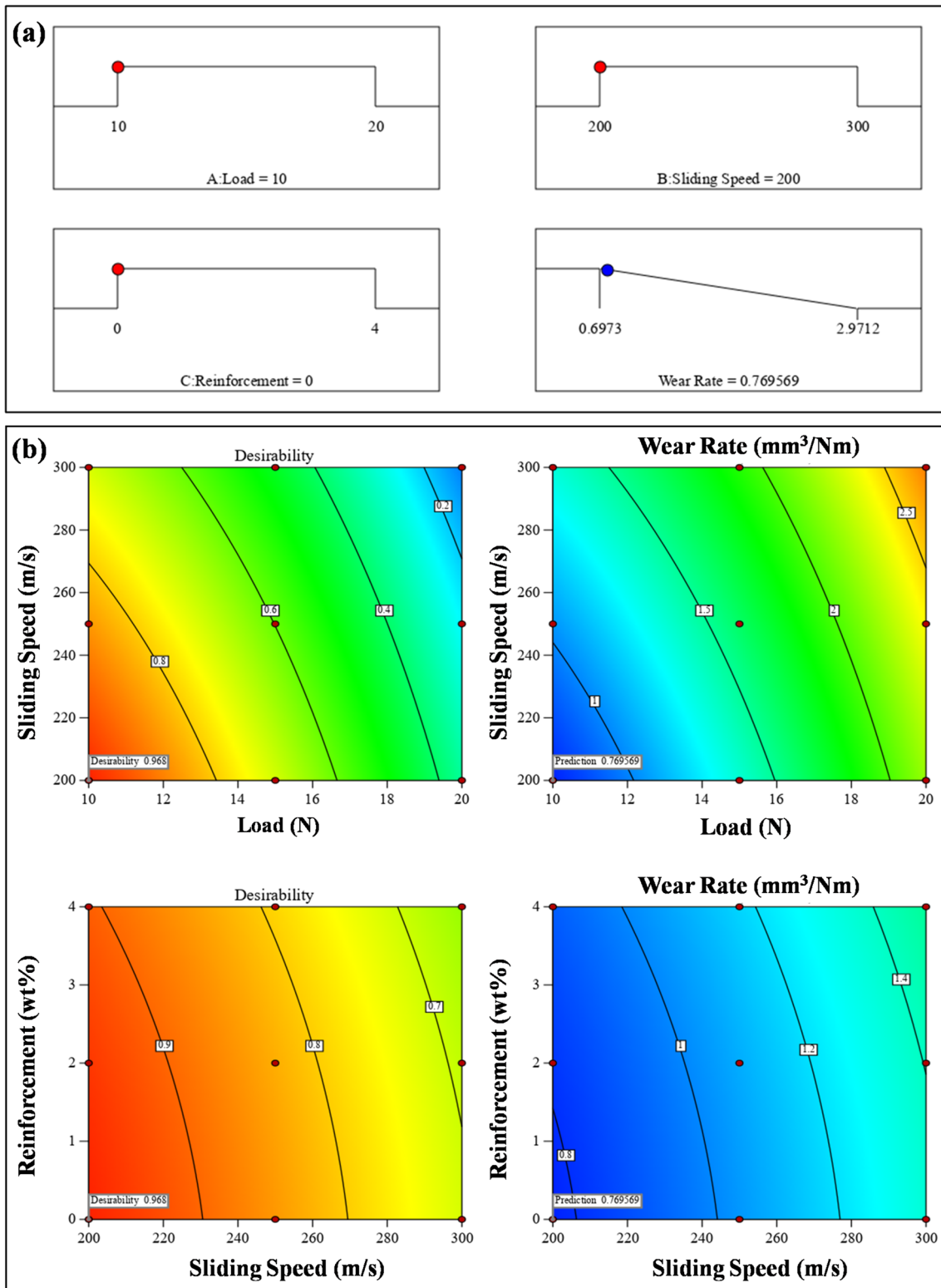
Fig. 9 **a** Ramp plots for optimized parameters of wear rate, and **b** Desirability plots for wear rate

Table 6 Confirmation test results at optimized condition

Load (N)	Sliding speed (rpm)	Reinforcement (wt %)	Predicted wear rate (mm³/Nm)	Observed wear rate (mm³/Nm)	Error (%)
10	200	0	0.7695	0.7481	2.86

wear resistance compared to the Al5052 alloy. Additionally, with the increase in wt.% reinforcement, wear resistance increases. Therefore, the 3D surface topography provides a suitable basis for comparing and correlating the surface roughness of test samples in worn surfaces under optimized conditions.

4 Conclusions

The investigation employed a manufacturing technique known as compo-casting to create composite materials consisting of Al5052 alloy combined with Cenosphere particles. The microstructural examination includes SEM and EDS analysis exhibiting a uniform dispersion of these particles throughout the composite material. Through XRD analysis, crucial components such as Al, Si, MgO, and $MgAl_2O_4$ were identified in both the Al5052 alloy and the composite materials. Furthermore, a graphical representation highlighted the distinct phases of cenosphere particles within the composite material, providing a visual insight into their distribution and behavior.
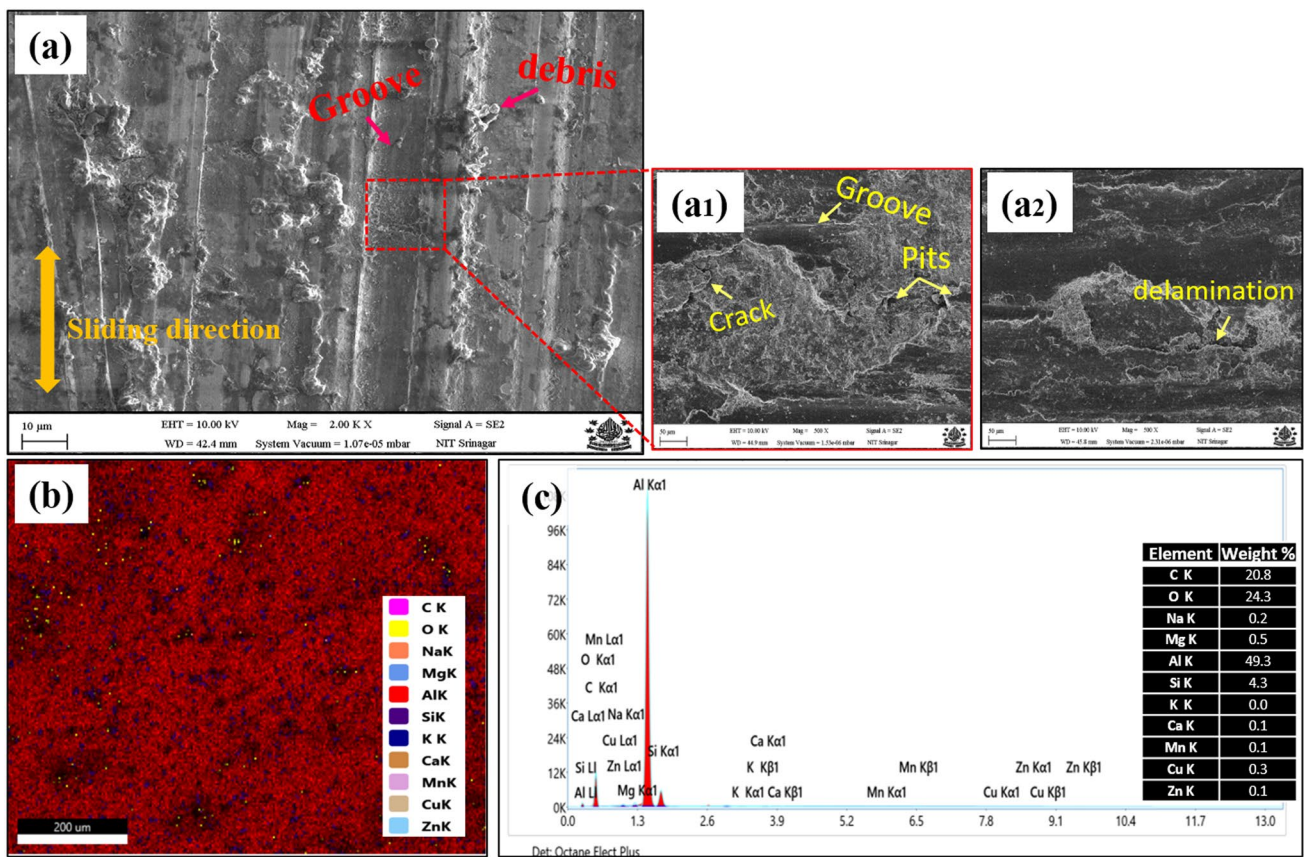
Fig. 10 Worn surfaces of Al5052 alloy; **a**, a1, a2 SEM micrographs, **b-c** EDS and elemental mapping
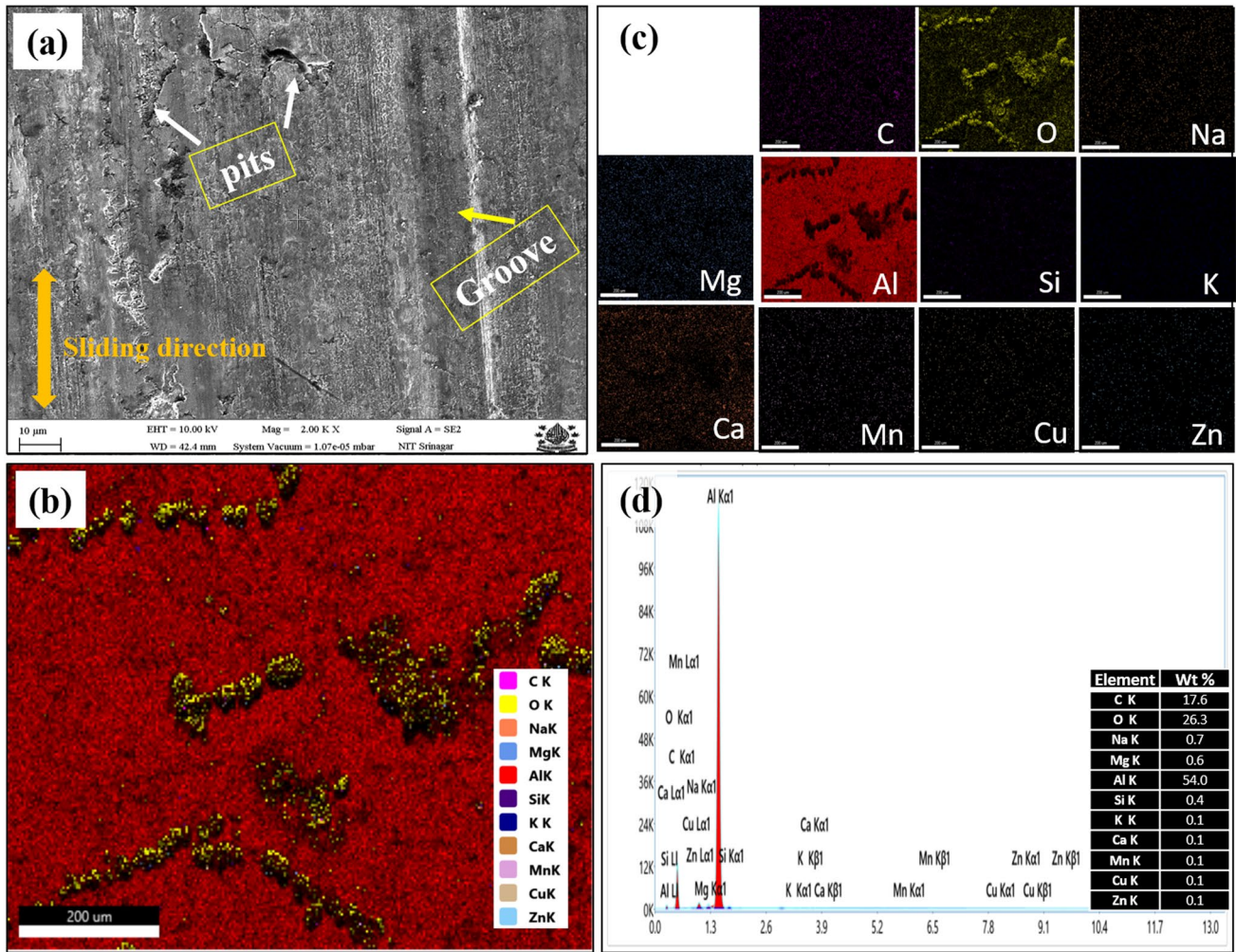
Fig. 11 Worn surfaces of Al5052 + 2 wt.% Cenosphere; SEM micrographs, **a** SEM micrograph, **b-d** EDS and elemental mapping
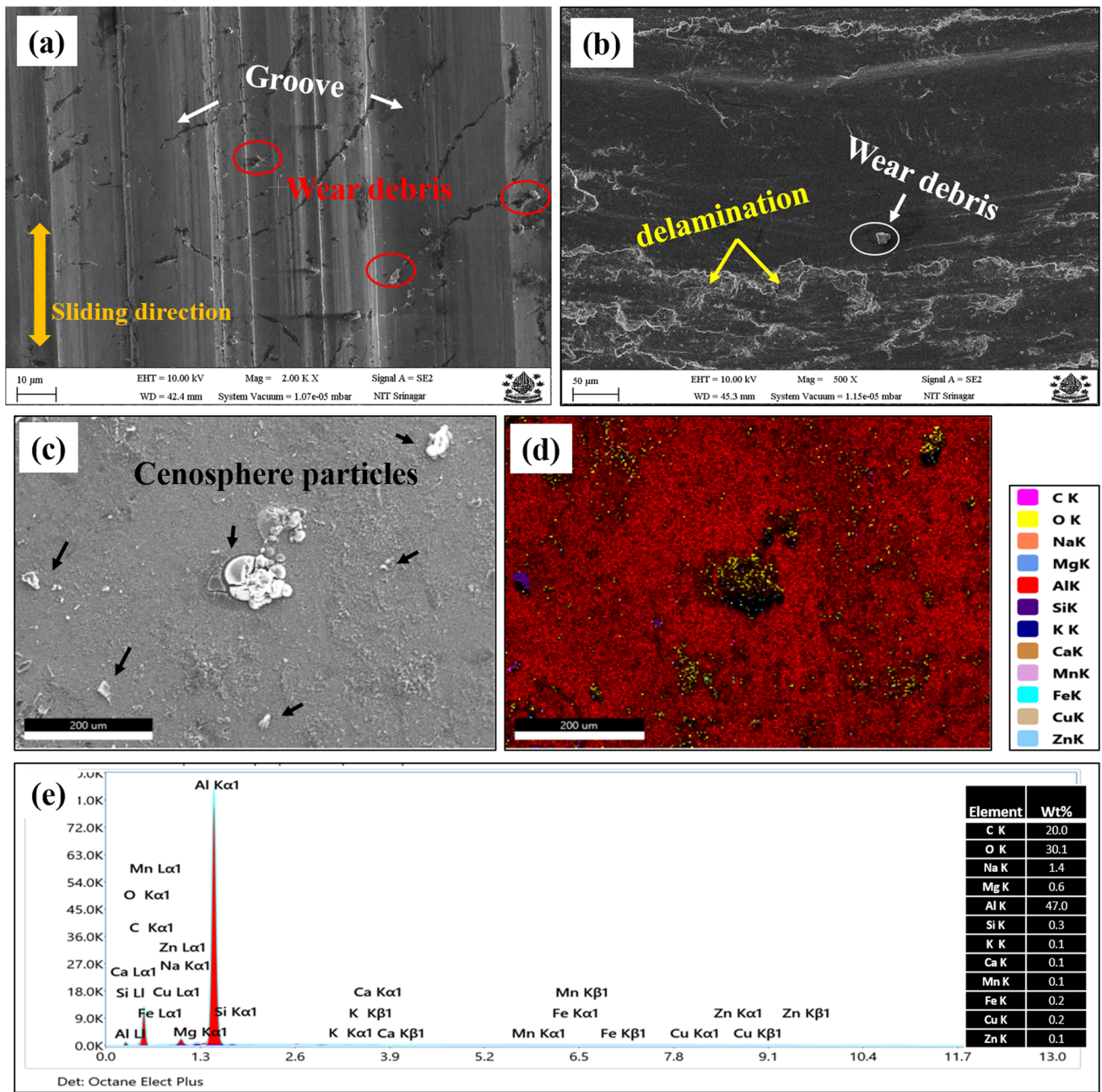
Fig. 12 Worn surfaces of Al5052 + 4 wt.% Cenosphere; **a-c** SEM micrographs, **d-e** EDS and elemental mapping
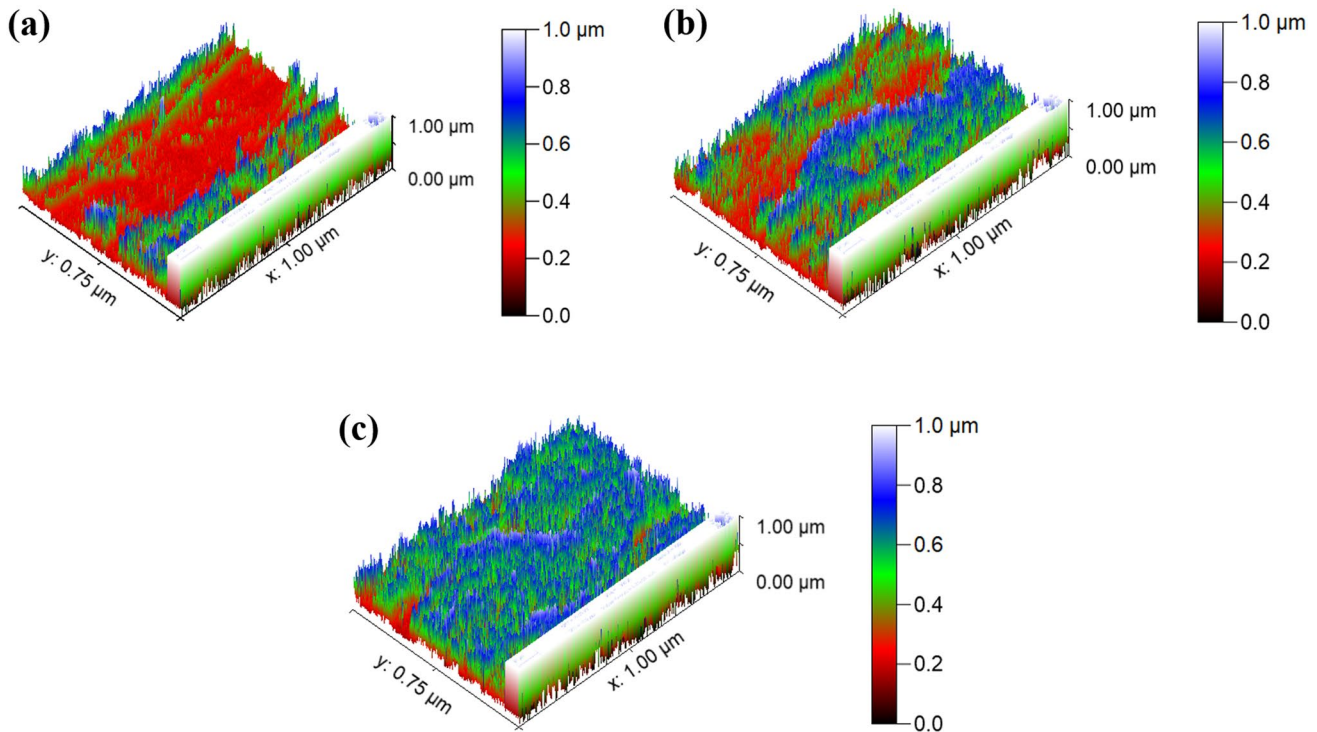
(a)

(b)

(c)

Fig. 13 3D surface topography of the worn surface of **a** Al5052 alloy, **b** Al5052 + 2 wt.% Cenosphere, and **c** Al5052 + 4 wt.% Cenosphere

- Utilizing the Response Surface Methodology's Central Composite Design module, optimization was conducted for load, sliding speed, and reinforcement weight. The model, boasting an R^2 value of 98.52%, pinpointed load, sliding speed, and the weight percentage of reinforcement as significant variables.
- Ramp plots delineated the optimal conditions: a load of 10 N, sliding speed of 200 rpm, and no reinforcement weight. Subsequent confirmation testing closely mirrored the projections, revealing a minor 2.86% deviation in wear rate.
- The incorporation of Cenosphere into the Al5052 matrix bolstered the composite's hardness, with the distribution of particles playing a critical role in characterization. Plastic deformation caused indentations on the worn surface, with plowing and delamination as primary wear mechanisms. Al5052 + 4 wt.%Cenosphere exhibited the lowest (Ra) surface roughness (1.05 μm^{-1}), indicating superior wear resistance compared to Al5052 alloy (Ra = 1.346 μm^{-1}).

Declarations

References

1. Sharma, P., *Prod. Technol.* S. Chand & Co. Ltd: NJ (2004)
2. Alloys E R, *Spec. Purpose Mater.* **15** (3), (1998) 95.
3. Mazahery A, and Shabani M O, *Powder Technol.* **217** (2012) 558–565.
4. Purohit R, Qureshi M, and Dandoutiya B K, *Mater Today Proc.* **5** (9), (2018) 20492–20499.
5. Kumar A, Lal S, and Kumar S, *J. Mater. Res. Technol.* **2** (3), (2013) 250–254.
6. Raju K, and Balakrishnan M, *Silicon* **23** (2020) 1.
7. Shabani M O, and Mazahery A, *Ceram. Int.* **38** (6), (2012) 4541–4547.
8. Kandpal B C, and Singh H, *Mater. Today Proc.* **4** (2), (2017) 2783–2792.
9. Zhiqiang S, Di Z, and Guobin L, *Mater. Des.* **26** (5), (2005) 454–458.
10. Rao R N, Das S, Mondal D P, and Dixit G, *Wear* **267** (9–10), (2009) 1688–1695. https://doi.org/10.1016/j.wear.2009.06.034
11. Das D, et al., *Mater. Today Proc.* **4** (2), (2017) 2965–2974.
12. Kishore P, Kumar PM, and Dinesh D, In *AIP Conference Proceedings*. AIP Publishing (2019)
13. Dey A, Debnath S, and Pandey K, *Trans. Nonferr. Metals Soc. China* **27** (5), (2017) 998–1010.
14. Reddy M, *J. Propuls. Technol.* **44** (2023) 5407–5417.

15. Rajan T, et al., *Compos. Sci. Technol.* **67** (15–16), (2007) 3369–3377.
16. Bharti S, Ghetiya N D, and Dutta V, *Mater. Today Proc.* **44** (2021) 52–57.